Proceedings of the 17th World Congress
The International Federation of Automatic Control
Seoul, Korea, July 6-11, 2008

Active Cardiac Stabilization using H_∞ Control Methodology

Wael Bachta * **Edouard Laroche** * **Pierre Renaud** **
Jacques Gangloff *

* *LSIIT (UMR CNRS-ULP 7005), Strasbourg I University, France*
{wael,laroche,jacques}@eavr.u-strasbg.fr
** *LGeCo, INSA-Strasbourg, France*
pierre.renaud@insa-strasbourg.fr

Abstract: Beating heart surgery is an important milestone in cardiac surgery. This technique is currently made possible thanks to the use of passive mechanical stabilizers. Nevertheless, the commercially available stabilizers exhibit significant residual motion, which is inherent to their geometry. Recently, a novel active stabilizer based on a compliant structure has been designed. High-speed visual feedback is used to compensate for the residual cardiac motion with a piezo actuator. In this paper three H_∞ control strategies with different levels of a priori knowledge on the disturbance are tested and compared. First, a classical feedback strategy without any assumption on the disturbance is designed. Second, a feedback control law with a resonant filter centered at the cardiac fundamental frequency is synthetized. Finally, a 2 degrees-of-freedom controller fed with a prediction of the heart motion is proposed. The prediction is obtained with an original method provided in this article.

Keywords: medical robotics, cardiac surgery, disturbance rejection, H_∞ control, preview

1. INTRODUCTION

1.1 Beating heart surgery context

Conventional Coronary Artery Bypass Grafting (CABG) with cardiopulmonary bypass allows the surgeons to operate on a motionless heart. However, the use of a heart-lung machine can cause deleterious effects on the neurological, renal and respiratory functions. In order to avoid such post-operative complications, the off-pump CABG has been proposed: the operation is then performed on a beating heart. Cardiac stabilizers, consisting in passive mechanical devices, are used for reducing the motion of the area of interest. In the even more challenging totally endoscopic CABG, all the surgical instruments are introduced into the patient body through small incisions of small diameter, typically 10 mm. The endoscopic cardiac stabilizers are composed of a long and thin arm equipped with a distal device allowing an accurate positioning on the heart. Due to their geometry, these stabilizers exhibit an important residual motion (Loisance et al. [2005], Cattin et al. [2004]) far below the estimated 0.1 mm accuracy required for the surgical gesture.

1.2 An active stabilizer

Over the years, many contributions have been proposed to deal with the cardiac motion compensation using an actuated system. One approach consists in displacing a robotized tool holder synchronously with the anastomosis site movement, without any contact (Thakral et al. [2001], Namakura et al. [2001], Ginhoux et al. [2005], Bebek et al. [2007]). Accurate tracking is obtained, but the high acceleration capacities of the robot are a danger for both the patient and the surgeon. A novel approach, considered herein, has been proposed by Bachta et al. [2007], allowing the separation of the stabilization and the surgical tasks. The stabilization is achieved using a novel device, the Cardiolock, which is an active cardiac stabilizer based on a compliant structure and a piezo actuator. A high-speed camera is used for measuring the displacements of the end-effector and high-speed visual servoing is performed to suppress any residual displacement of the beating heart surface.

1.3 Disturbance rejection

The heart motion acts on the stabilizer as a disturbance. Thanks to the heart motion repeatability, a prediction of the future disturbance values can be processed. Model Predictive Control is a standard approach allowing to take into account a prediction and has therefore been extensively used in this context (Ginhoux et al. [2005], Bebek et al. [2007]). In our application, we propose to use H_∞ control strategies for two reasons:

- H_∞ control strategies are well known for their robustness properties. In our case, robustness issues are twofold: First, the dynamics of the system evolve, due to the contact with the heart. Second, a finite dimension model is used to describe the mechanism flexibilities.
- The system contains flexible modes with low damping that can be well handled by a H_∞ controller.

Different H_∞ control strategies can be considered, depending on the level of knowledge of the disturbance. In this paper, we propose and compare three control schemes. In a first approach, a simple feedback controller is designed,

without any assumption on the disturbance nature. Then, the a priori fundamental cardiac frequency value is used during the design of a second controller. Finally an H_∞ controller with preview is synthetized. This implies a prediction model of the cardiac motion, which is provided in this article with a novel method of heart motion prediction. This paper is organized as follows: in Section 2 the active stabilizer is introduced, with its dynamic modeling and a new prediction method. In section 3, the three H_∞ control strategies are presented. Simulation results are given with the comparison of their efficiencies. Finally, the respective interest of the three approaches are discussed before concluding.

2. DESCRIPTION AND MODELING

In this section, a description of the proposed active stabilizer is provided. A dynamic model of the mechanism and the visual loop used to control the device is then derived. Finally, a new prediction method which will be used for control purposes is introduced.

2.1 System description

The proposed prototype allows currently to compensate for residual displacement in one single direction corresponding to the maximum encountered cardiac force and motion. The device consists of two parts (fig. 1). A first active part is composed of a one degree-of-freedom (DOF) closed-loop mechanism remaining outside the patient body in a totally endoscopic surgery context. The other part is a beam of 10 mm diameter and 300 mm length. Figure 1 shows that the closed-loop mechanism is composed of a piezo actuator (Cedrat Technologies) and three revolute compliant joints. The closed-loop mechanism is designed as a compliant slider-crank system, enabling the transformation of the piezo actuator linear displacement in a rotation motion. The piezo actuator is connected to a driver including a power amplifier and a local deformation control loop using a strain gauge measurement. Using this driver, it is possible to accurately control the displacement with a quasi-linear transfer function.
The compensation principle is decomposed in two sequential steps on figure 2: on the top, one can see a magnified deflection due to an external load, and on the bottom the cancellation of the tip displacement by modifying the geometry of the closed-loop mechanism. On the current

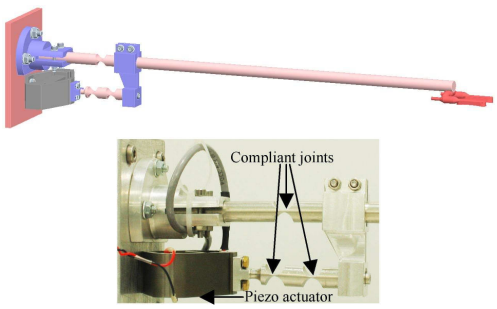

Fig. 1. The current prototype of the active stabilizer. On the top, a CAD global view and on the bottom the detail of the closed-loop mechanism on the current prototype

prototype, the position of the distal end is obtained with a 333 Hz camera with a resolution of 128 pixels per mm.

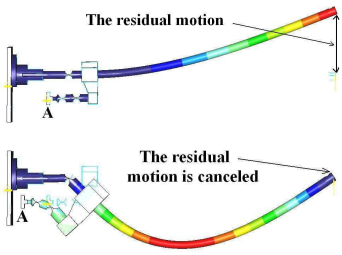

Fig. 2. A finite element analysis of the compensation. The actuator controls the horizontal position of the point A. Displacements are magnified for the sake of clarity

2.2 Dynamic modeling of the mechanism

The proposed flexible active cardiac stabilizer is modeled using the Pseudo Rigid Body Model (PRBM) approach (Howell [2001]). In this approach, flexure hinges are approximated by classical joints associated with torsion springs K_r describing the material elasticity (fig.3). In the same way, the deflection of a cantilever beam can be modeled by a rotating rigid beam with a torsion spring K_l. In this system one DOF is controlled by the piezo actuated

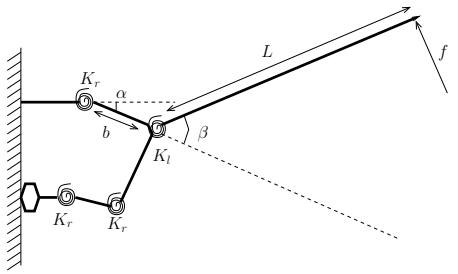

Fig. 3. The PRBM of the device with an external force

closed loop structure, and one DOF which corresponds to the rotation of the distal beam of length L is non actuated. Thus the active stabilizer can be approximated by a 2-link flexible serial robot. The first arm is modeled by a beam of length b which position is defined by an angle α, while the second arm is the distal beam which position is described by an angle β.
Thanks to the fast response of the piezo actuator, we can consider that the angle α is controlled with a high bandwidth compared to the dynamics of the deflection. This is equivalent to consider that the angle α is equal to the reference signal α^* sent to the piezo driver. Therefore, α is considered as an input of the system and the dynamic model of the system can be reduced to a single equation:

$$M_{21}\ddot{\alpha} + M_{22}\ddot{\beta} + C_2(\alpha, \beta, \dot{\alpha}, \dot{\beta}) = \Gamma_2 \qquad (1)$$

where: $M_{21} = I_2 + \frac{1}{4}m_2L^2 + \frac{1}{2}m_2bL\cos\beta$, $M_{22} = I_2 + \frac{1}{4}m_2L^2$, $C_2 = \frac{1}{2}m_2bL\dot{\alpha}^2\sin\beta$ and $\Gamma_2 = Lf - K_2\beta - f_2\dot{\beta}$. m_2 and I_2 are respectively the weight and the inertia moment of the second arm. K_2 and f_2 describe the stiffness and the material friction of the second arm. f describes the applied cardiac force. As only small displacements are

involved, the equation can be linearized around a nominal position ($[\alpha, \beta, \dot{\alpha}, \dot{\beta}] = [0, 0, 0, 0]$). Finally, a linear model can be written as:

$$M_{22}\ddot{\beta} + f_2\dot{\beta} + K_2\beta = Lf - M_{21}\ddot{\alpha} \quad (2)$$

For small displacements, the stabilizer tip position can be expressed as:

$$y = (b + L)\alpha + L\beta \quad (3)$$

Using (2), (3) and the Laplace variable s, we can write in the frequency domain:

$$Y(s) = \mathrm{G}(s)\alpha(s) + \mathrm{P}(s)F(s) \quad (4)$$

with:

$$G(s) = \frac{((b + L)M_{22} - LM_{21})s^2 + (b + L)(f_2 s + K_2)}{M_{22}s^2 + f_2 s + K_2} \quad (5)$$

and:

$$P(s) = \frac{L^2}{M_{22}s^2 + f_2 s + K_2} \quad (6)$$

2.3 Modeling of the visual loop

Figure 4 shows a block diagram of the visual loop. The computed control u signal is converted into an analog voltage with a digital to analog conversion modeled by a Zero Order Holder (ZOH). This voltage corresponds to the reference of the piezo servoing loop α^*. Due to the high dynamics of this loop, we assume that $\alpha^* = \alpha$. The output y is measured using the position of a visual marker v in the image given by a high speed camera with a sampling period $T_s = 3\,\mathrm{ms}$. The dynamic effect of the camera can be modeled as an averaging filter representing the exposure time effect. The camera model C_m can be, be written (Ranftl et al. [2007]) as $\mathrm{C}_m(z) = \frac{1+z^{-1}}{2}$.
A time delay of one period is required for the acquisition and the processing of the current image.
Finally, for control purposes, the model of figure 4 is simplified to get the diagram of figure 5. The signal p represents an equivalent output disturbance expressed in pixels, and $\mathrm{H}(s)$ is the bilinear transform of $\mathrm{H}(z)$, with:

$$\mathrm{H}(z) = (1 - z^{-1})\mathcal{Z}\{\frac{G(s)}{s}\}\mathrm{C}_m(z)z^{-1} \quad (7)$$

As a conclusion of this section, figure 6 represents a bode magnitude plot of $\mathrm{H}(s)$ describing the transfer between the control signal and the visual measurement. The bandwidth of the obtained system is 78 Hz and we can observe the low damping of the resonance.

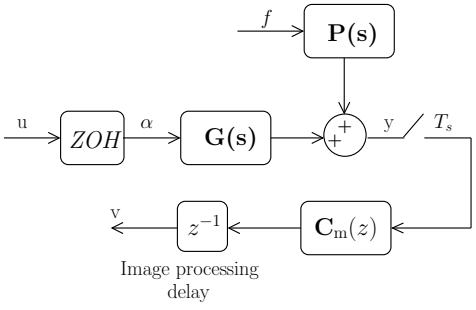

Fig. 4. A diagram of the plant model

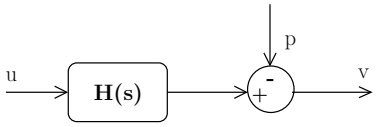

Fig. 5. A block diagram of the controlled plant

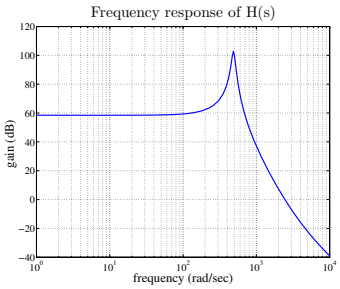

Fig. 6. A bode magnitude plot of $\mathrm{H}(s)$

2.4 Disturbance prediction algorithm

Figure 7 shows a pig heart motion when stabilized with a passive stabilizer (Bachta et al. [2007]). This motion is composed of two periodic components. The large amplitude and slow frequency motion $\mathcal{M}_r$ is the influence the respiration. The medium amplitude and faster component $\mathcal{M}_c$ is due to the heartbeats. The disturbance can be written as:

$$p(k) = \mathcal{M}_c(k) + \mathcal{M}_r(k) \quad (8)$$

where k is the current sample number. Let f_c and f_r be respectively, the frequencies of the cardiac and respiratory signals. ϕ_c and ϕ_r are the associated phases. Denoting T_s the sampling period, these phases are updated as follows:

$$\begin{cases} \phi_c(k) = \phi_c(k-1) + 2\pi f_c T_s \\ \phi_r(k) = \phi_r(k-1) + 2\pi f_r T_s \end{cases} \quad (9)$$

The cardiac and respiratory frequencies can be measured online using biological data. The former is acquired by detecting the QRS complex occurrences of the ECG signal. The latter is extracted from the ventilation flow given by airflow sensors.
In the classical modeling approaches proposed in the literature, no coupling between the respiratory and the cardiac motions is taken into account. Therefore, based on the periodic behaviour of the respiratory and cardiac motions, it can be written:

$$\mathcal{M}_r(k) = \sum_{i=1}^{n_r} \Big(a_{ri} \sin\big(i\phi_r(k)\big) + b_{ri} \cos\big(i\phi_r(k)\big) \Big) \quad (10)$$

In the same way:

$$\mathcal{M}_c(k) = \sum_{i=1}^{n_c} \Big(c_{ci} \sin\big(i\phi_c(k)\big) + d_{ci} \cos\big(i\phi_c(k)\big) \Big) \quad (11)$$

where n_c and n_r are respectively the number of cardiac and respiratory harmonics, a_{ri}, b_{ri}, c_{ci} and d_{ci} are the Fourier coefficients.
The estimation of the two motion components for prediction purposes has been achieved through different techniques in the literature e.g adaptive filtering in Ginhoux et al. [2005] or Fourier coefficients estimation in Thakral et al. [2001].

The coupling between the two motion components is outlined in Cuvillon et al. [2005] and integrated in a Linear Parameter Varying model (LPV) of the heart motion. The presented method, even giving good results, needs an explicit separation of the two motion components in order to identify the model parameters. Moreover, a change in the physiological parameters (respiratory or heartbeat frequency) implies a re-initialization of the algorithm.
Hereafter, we propose an alternate method to take into account in a simpler way the coupling between the two components while remaining in the Fourier coefficient estimation framework. Indeed, the cardiac motion is expressed as as an amplitude modulation where the carrier is a cardiac signal $\mathcal{C}_c$:

$$\mathcal{C}_c(k) = \sum_{i=1}^{n_c} \Big(e_{ci} \sin\big(i\phi_c(k)\big) + f_{ci} \cos\big(i\phi_c(k)\big) \Big) \qquad (12)$$

with n_c the number of cardiac harmonics, e_{ci} and f_{ci} the Fourier coefficients. The modulated signal is a respiratory one expressed as:

$$\mathcal{C}_r(k) = \sum_{i=1}^{n_r} \Big(g_{ri} \sin\big(i\phi_r(k)\big) + h_{ri} \cos\big(i\phi_r(k)\big) \Big) \qquad (13)$$

with n_r the number of respiratory harmonics, g_{ri} and h_{ri} the Fourier coefficients.
Therefore the new cardiac motion can be given by:

$$\mathcal{M}_c(k) = \mathcal{C}_c(k)(1 + \mathcal{C}_r(k)) \qquad (14)$$

In order to keep a linear model, all the products of terms e_{ci}, f_{ci}, g_{ri} and h_{ri} are replaced with new terms. Using this linearization and (8), we can write:

$$p(k) = \mathbf{x}^T \ \Phi(k) \qquad (15)$$

where $\mathbf{x}$ is the parameters vector to be estimated, and $\Phi(k)$ the regression vector at sample time k.
Using equation (15), the parameter vector is updated at each sample by a Recursive Least Squares (RLS) algorithm with a forgetting factor. If the current disturbance value $p(k)$ is not measurable, as herein, it can be estimated using an appropriate disturbance observer. As the regression vector can be computed several samples ahead, and using the obtained model, it is possible to predict the cardiac motion. The standard deviation of the current sample estimation error after the parameters convergence is 1.9 pixels. Figure 7 shows four samples ahead cardiac prediction results. The standard deviation after the parameters convergence is 2.1 pixels, which shows good prediction properties of the derived model. These two results are given for $n_c = 10$ and $n_r = 4$.

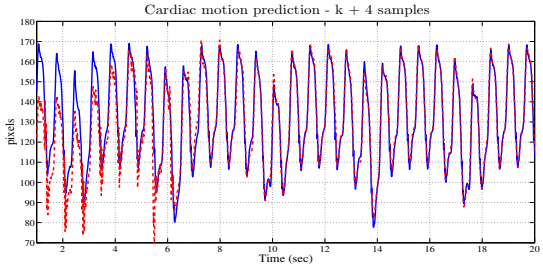

Fig. 7. The cardiac motion prediction four samples ahead (cardiac motion in blue line, prediction in dotted red line)

3. H_∞ CONTROL

The stabilization task consists in designing an appropriate feedback control law that cancel the displacement caused by the cardiac force f. In the following, three different H_∞ control schemes are proposed and compared.
The control laws are designed in continuous time and converted into discrete-time with the bilinear transform for implementation. Discrete time synthesis could also have been used.

3.1 One Degree-of-Freedom Controller

For output disturbance rejection problem, a two-blocks synthesis scheme can be used as illustrated in figure 8. The controller synthesis relies on two weighting functions W_1 and W_3. The controller $K(s)$ is designed in order to minimize the H_∞ norm of the performance channel (the transfer between $w = [r]$ and $z = [z_1, z_2]$). The control loop bandwidth and modulus margin are defined by the frequency behavior of T_{ep}. Therefore, we have chosen

$$W_1(s) = \frac{\frac{s}{M} + \omega_{cr}}{s + E_p \omega_{cr}} \qquad (16)$$

where $\frac{1}{M} = 0.5$ is the required modulus margin, $E_p = 10^{-4}$ is the maximum allowed steady error and $\omega_{cr} = 400 \ \mathrm{rad\,s^{-1}}$ is the desired closed loop bandwidth.
In order to allow the roll-off effect in high frequencies, we have chosen:

$$W_3(s) = \frac{1}{k_3} \frac{k_3 s + \omega_{cr}}{K_3 s + \omega_{cr}} \qquad (17)$$

where $K_3 = 3$, $k_3 = 10^{-4}$ and $\omega_{cr} = 500 \, \mathrm{rad\,s^{-1}}$ is the radial frequency beyond which the gain is attenuated.
The obtained performance index is $\gamma = 2.3137$. Figure 9 shows the resulting closed loop transfers and their respective templates.
Figure 14 shows the resulting steady error of a temporal simulation test using experimentally recorded disturbance data. The standard deviation of the steady residual motion is 1.5 pixel.

3.2 One degree-of-freedom controller with a resonant filter

With the previous approach, the respiratory component of the disturbance is completely suppressed because of its low frequency, whereas the cardiac component is only partially filtered. Figure 15 shows a frequency analysis of the error. The dominant contribution corresponds to the cardiac frequency. Therefore, a the weighting function W_1 is multiplied by a notch filter, in order to attenuate this

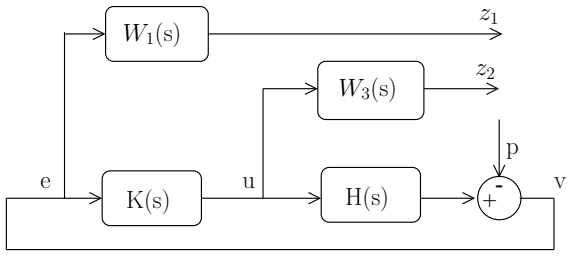

Fig. 8. A 1 DOF controller, 2 blocks augmented plant

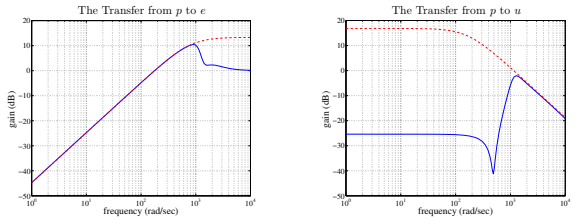

Fig. 9. One DOF controller synthesis (templates in dotted red line, obtained transfers in blue line)

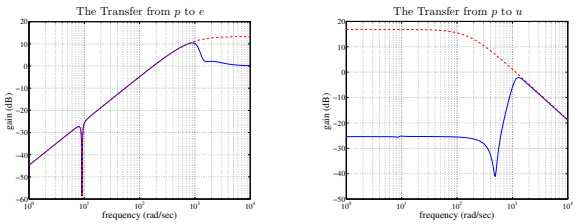

Fig. 10. One DOF controller with resonant filter (templates in dotted red line, obtained transfers in blue line)

disturbance component with more efficiency. This notch filter is the inverse of a band stop filter centered around the cardiac frequency which allows a more significant attenuation in a narrowband around this frequency. The transfer function of such a filter is given by:

$$T = \frac{s^2 + 2\zeta_{\text{num}} s + \omega_c^2}{s^2 + 2\zeta_{\text{den}} s + \omega_c^2} \tag{18}$$

where w_c is the fundamental cardiac angular frequency, and $\zeta_{\text{num}} > \zeta_{\text{den}} \in [0, 1]$. The ratio between ζ_{den} and ζ_{num} defines the amplification around w_c. It is worth noticing that higher values of ζ_{den} provides less sensitivity to the uncertainty on ω_c. Hereafter, $\zeta_{\text{num}} = 0.45$, $\zeta_{\text{den}} = 0.01$ and $\omega_c = 9.1\,\text{rad}\,\text{s}^{-1}$

The obtained performance index is $\gamma = 2.3154$. Figure 10 shows the resulting closed loop transfers and their respective templates.

Using the same data, the result of a temporal validation is given in fig. 14. The standard deviation is reduced to 1 pixel. Figure 15 shows a significant attenuation at the fundamental cardiac frequency component.

3.3 Two Degree-of-Freedom Controller

Taking into account future disturbances enhance the control loop performances. Since an efficient prediction method has been proposed in subsection 2.4, a two-degree-of-freedom control scheme with preview capabilities is considered (fig.11). The proposed controller consists of two parts: a feedback and a feedforward terms. These two parts are designed simultaneously.

Only proper transfer functions are permitted in classical H_∞ controller design algorithms. Therefore, in the design scheme shown in fig.12, the preview term fed into the feedforward channel is transformed into a delay approximated with its Pade model $D(s)$.

After deriving the augmented plant, a controller is designed to minimize the H_∞ norm of the transfer between $w = [r, p]$ and $[z_1, z_2]$. This corresponds to a classical four blocks scheme. For a fair comparison, the adopted

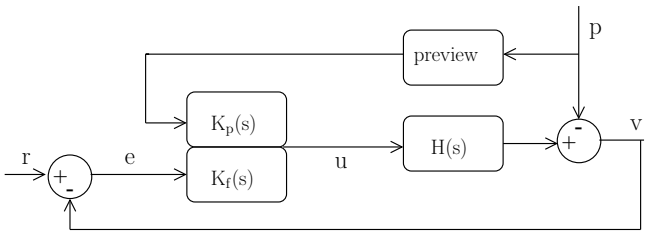

Fig. 11. A two DOF controller with a preview term

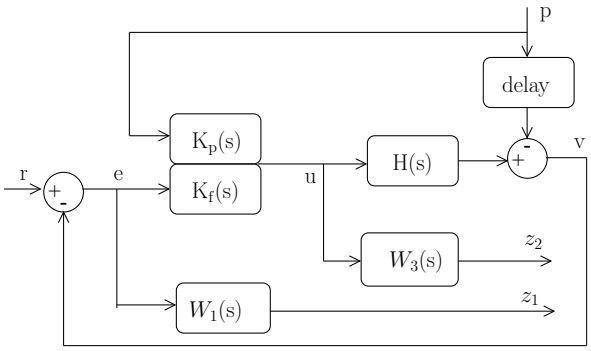

Fig. 12. The augmented plant corresponding to the two DOF controller with preview

weighting functions are the same as for the one degree of freedom controller without the notch filter.

The obtained performance index is $\gamma = 2.3110$. Figure 13 shows the resulting closed loop transfers and their respective templates.

Figure 14 shows the steady error given by a temporal simulation when a four steps ahead exact preview term (i.e equal to the system order) is involved. The standard deviation of steady error is 0.5 pixel. Figure 15 shows that the frequency content of the error is strongly attenuated thanks to the prediction.

A second simulation has been performed using the two DOF controller. In that case, an estimation of the preview term is fed into the controller. Figure 14, shows the resulting steady error. The standard deviation of the error is then equal to 0.8 pixel. This performance slight decrease is probably due to the prediction error.

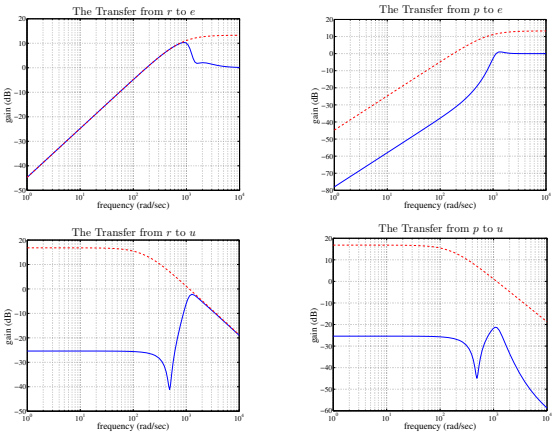

Fig. 13. Two DOF controller (templates in dotted red line, obtained transfers in blue line)

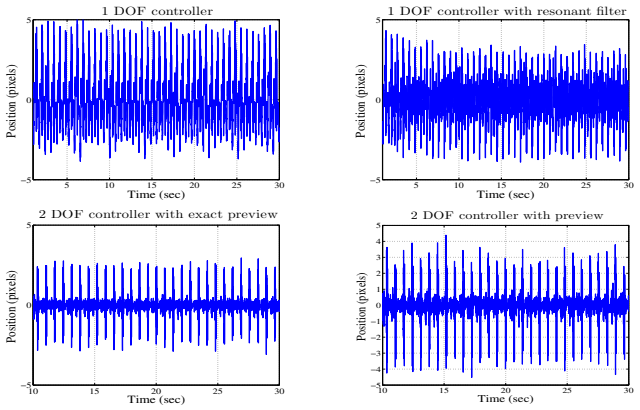

Fig. 14. The steady residual motion using the different controllers

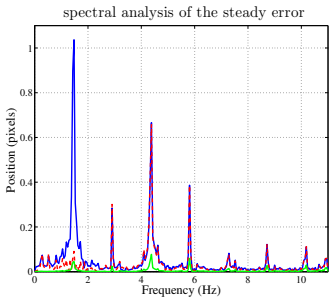

Fig. 15. Frequency analysis of the steady error (1 DOF control in solid blue line, 1 DOF with resonant filter in red dotted line, 2DOF with exact preview in solid green line)

3.4 Discussion

The standard deviations of the resulting steady errors when using the three control schemes are summarized in table 1. The three controllers give satisfying results since the peak-to-peak error is below 13 pixels which corresponds to 0.1 mm, the required accuracy. However due to the high sensor resolution, every little decrease in the error amplitude represents a great improvement in the stabilization quality. Hereafter the benefits and shortcomings of the three proposed strategies are addressed. The advantage of the standard one DOF controller is that no particular knowledge of the disturbance characteristics is needed during the design process. This is an interesting feature because the biological data vary with respect to the patients. The one DOF controller with a resonant filter improves the final result. However the synthesis requires a prior knowledge of the cardiac frequency. This shortcoming could be cut off if an LPV control framework was considered. Notice that this approach implies a significant increase of the controller order if all the disturbance harmonics have to be taken into account. Finally, the best results are obtained using the two DOF controller with preview capabilities. This strategy requires a prediction model of the disturbance but no physiological information is needed during the synthesis. This approach is sensitive to the prediction errors. Significant prediction errors could occur if some arrhythmia happen during the surgical intervention.

1 DOF classical feedback	1.5
1 DOF with notch filter	1
2 DOF with exact preview	0.5
2 DOF with prediction	0.8

Table 1. The standard deviation (in pixel) of the steady error using the three controllers

4. CONCLUSION

In this paper, the active cardiac stabilization problem is addressed from a control point of view. After describing the medical device and deriving a dynamic model of the system including the visual sensor, an original cardiac motion prediction method has been introduced. Three different H_∞ control strategies have then been compared. Future work will now include the experimental validation of the proposed approaches, that will allow further comparisons of the control schemes.

REFERENCES

W. Bachta, P. Renaud, E. Laroche, J. Gangloff and A. Forgione. Cardiolock : an active cardiac stabilizer, fisrt in vivo experiments using a new robotized device *In Medical Image Computing and Computer-Assisted Intervention - MICCAI*, 2007

O. Bebek and M.C. Cavusoglu. Intelligent Control Algorithms for Robotic-Assisted Beating Heart Surgery. *IEEE Transactions on Robotics*, Vol.23, No. 3, pp. 468-480, 2007.

P. Cattin, H. Dave, J. Grünenfelder, G. Szekely, M. Turina and G. Zünd. Trajectory of coronary motion and its significance in robotic motion cancellation. *European Journal of Cardio-thoracic Surgery*, vol. 25, pp 786-790, 2004.

L. Cuvillon, J. Gangloff, M. de Mathelin and A. Forgione, Toward robotized Beating heart TECABG : assessment of the heart dynamics using high-speed vision. *In Medical Image Computing and Computer-Assisted Intervention - MICCAI*, pp. 551-558, 2005.

R. Ginhoux, J.A. Gangloff, M.F. de Mathelin, L. Soler, M.M.A Sanchez and J. Marescaux. Active Filtering of Physiological Motion in Robotized Surgery Using Predictive Control. *IEEE Transactions on Robotics*, Vol.21, No. 1, pp. 67-79, 2005.

L.L. Howell. Compliant mechanisms *Wiley-IEEE*, 2001

D.Y. Loisance, K. Nakashima and M. Kirsch. Computer-assisted coronary surgery: lessons from an initial experience. *Interactive Cardiovascular and Thoracic Surgery*, Vol. 4 pp 398-401, 2005

Y. Nakamura, K. Kishi and H. Kawakami. Heartbeat synchronization for robotic cardiac surgery. *IEEE Int. Conf. on Robotics and Automation*, vol. 2, pp. 2014-2019, 2001.

A. Ranftl, L. Cuvillon, J. Gangloff and J. Vander Sloten. High Speed Visual Servoing with Ultrasonic Motors *IEEE Int. Conf. on Robotics and Automation*, pp. 4472-4477, 2007.

A. Thakral, J. Wallace, D. Tomlin, N. Seth and N. V. Thakor. Surgical motion adaptive robotic technology (S.M.A.R.T): Taking the motion out of physiological motion. *In MICCAI01*, vol. 2208, pp. 317-325, Springer, 2001.